ResearchGate

See discussions, stats, and author profiles for this publication at: https://www.researchgate.net/publication/305384074

Active and Passive CT for waste assay using LaBr3(Ce) detector

Article *in* Radiation Physics and Chemistry · July 2016

DOI: 10.1016/j.radphyschem.2016.07.013

CITATIONS
0

READS
38

4 authors, including:

Tushar Roy
Bhabha Atomic Research Centre
23 PUBLICATIONS **47** CITATIONS
SEE PROFILE

Jilju Ratheesh
Bhabha Atomic Research Centre
3 PUBLICATIONS **3** CITATIONS
SEE PROFILE

Amar Kumar Sinha
Birat Medical college Teaching hospital, Nepal
73 PUBLICATIONS **492** CITATIONS
SEE PROFILE

Some of the authors of this publication are also working on these related projects:

DST project View project

All content following this page was uploaded by Tushar Roy on 30 November 2016.

The user has requested enhancement of the downloaded file. All in-text references underlined in blue are added to the original document and are linked to publications on ResearchGate, letting you access and read them immediately.

Radiation Physics and Chemistry 130 (2017) 29–34

Contents lists available at ScienceDirect

Radiation Physics and Chemistry

journal homepage: www.elsevier.com/locate/radphyschem

Active and passive CT for waste assay using $LaBr_3(Ce)$ detector

Tushar Roy*, M.R. More, Jilju Ratheesh, Amar Sinha

Neutron & X-Ray Physics Division, Bhabha Atomic Research Centre, Mumbai, India

HIGHLIGHTS

- Use of $LaBr_3(Ce)$ for passive CT of ^{239}Pu has been reported for the first time.
- The passive data has been reconstructed using MLEM algorithm.
- Three dimensional distribution of ^{239}Pu is being reported.

ARTICLE INFO

Article history:
Received 4 April 2016
Received in revised form
12 July 2016
Accepted 13 July 2016
Available online 15 July 2016

Keywords:
Active and passive computed tomography
Plutonium
Lanthanum bromide

ABSTRACT

An active and passive computed tomography system has been developed that localizes and quantifies ^{239}Pu in a waste drum. The active (transmission) measurement uses an external gamma source and $LaBr_3(Ce)$ detector to determine the attenuation map of waste drum contents at different selected energies. The passive (emission) measurement uses multiple $LaBr_3(Ce)$ detectors to record the spectra of gamma-rays emitted from within the drum. The active and passive data sets are then coupled to quantitatively assay drum contents for ^{239}Pu.

© 2016 Elsevier Ltd. All rights reserved.

1. Introduction

Since the introduction of Computed Tomography (CT) (Herman, 1980; Kak and Slaney 1987), this technique has been used with different kinds of radiation sources for a large variety of imaging applications. The aim of transmission CT is to find the distribution of attenuation map within the volume of the given object. The transmission CT techniques have reached a very high stage of maturity with the development of new and improved technologies. These techniques are being routinely used for both clinical and industrial applications. However, in certain applications involving radionuclides, not only the spatial distribution but also the source strength is needed. Non-destructive burnup measurement of fuel assembly and waste assay are some examples of such application.

For waste drum application, Lawrence Livermore National Laboratory, USA had used HPGe detectors for scanning high level waste drums (Roberson et al., 1998; Camp et al., 2002). Similarly, some commercial tomographic gamma scanning systems using a single HPGe for waste drum assay are also available. However, the regulatory requirements now mandate characterization of not only high level waste but also a variety of nuclear wastes from low level waste drums to waste packets in small sizes. HPGe detector, besides being costly, is also bulky and need special cooling arrangements. For multi-detector applications which are required for fast scanning of drums for increased throughput and fast qualitative examination of thousands of such radioactive waste drums, the option of using multiple HPGe becomes very costly. Due to this, for several applications there is a need for alternate compact systems which are less cumbersome, can be used for field applications and at the same time give reasonable SPECT images. Recently, development of cerium activated lanthanum bromide ($LaBr_3(Ce)$) scintillators which have a better energy resolution than their other inorganic counterparts have prompted the need to explore its use for spectroscopy of complex energy spectra. Roy et al. (2013) have reported the application of $LaBr_3(Ce)$ for three dimensional SPECT imaging of ^{137}Cs. $LaBr_3(Ce)$ detectors have the advantage of a better resolution and a higher efficiency as compared to NaI(Tl) detectors. Although energy resolution is poorer than HPGe detectors, $LaBr_3(Ce)$ detectors are less costly, can be used for field or on-site applications and, since it does not require cryogenic cooling, large number of such detectors can be easily configured in various scanning geometries (Roy et al., 2015) and included in sophisticated systems.

In this paper, $LaBr_3(Ce)$ detectors have been used for SPECT imaging of ^{239}Pu in a mock waste drum. The 414 keV peak of ^{239}Pu

* Corresponding author.
E-mail address: tushar@barc.gov.in (T. Roy).

http://dx.doi.org/10.1016/j.radphyschem.2016.07.013
0969-806X/© 2016 Elsevier Ltd. All rights reserved.

can be easily distinguished in the complex plutonium spectrum and has been used for tomographic imaging. The use of $LaBr_3(Ce)$ detectors give an alternative to HPGe detectors for applications where fast scanning of Pu-bearing low level waste drums is required.

2. Active and passive computed tomography (A&PCT)

Active and passive computed tomography (A&PCT) (Camp et al., 2002; Roberson et al., 1998) is one of the most efficient techniques for characterization and localization of radioisotopes in nuclear waste assay. The A&PCT method consists of two steps to perform an assay: active CT and passive CT.

2.1. Active CT (Transmission CT)

In active CT, attenuation map of the object is obtained. This is similar to conventional X-ray CT but it uses an external gamma source (instead of X-ray) and the spectrum is recorded using a multi channel analyzer to discriminate between photons of different energies. It differs from conventional CT in that the energy of the external source should be different from the energy of the emitted gamma of the radioisotope source inside the object. Since the attenuation map has to be obtained for energy of the emitted gamma of the radioisotope source, the external gamma source used for active CT has, generally, multiple emission energies. The reconstructed CT images represent the linear attenuation coefficient of the object at specific energies. Energy specific attenuation maps are then used to determine the attenuation map of the object corresponding to the emission energy of the radioisotope to be imaged by interpolating the above data. Note that active CT neither identifies any isotope nor measures the source strength or activity within a waste drum.

2.2. Passive CT (Emission CT)

In the case of Passive CT (also called Single Photon Emission Computed Tomography or SPECT), the absorption of the gamma photon as it travels from the source to the detector has to be taken into account. In the absence of absorption, the problem simply reduces to reconstructing the source term from its measured Radon transform. In the presence of absorption, however, the exponential attenuation of the gamma rays inside the object has to be considered (Fig. 1). The source term is then reconstructed from the so-called *exponential Radon transform* or *attenuated Radon transform* (Novikov, 2002).

The reconstructed function in passive CT is the measured gamma-ray activity at one or more energies of all detectable radioisotopes within the object. The detection system collects the entire energy spectrum for each integration point and the radioisotopes are identified by their characteristic peaks within the energy spectrum.

2.3. Coupling active and passive CT

The data collected in the passive CT step is used to reconstruct the source activity corresponding to one or more gamma energies of the radioisotope(s). The energy dependent attenuation suffered by the photons in travelling inside the object is corrected by suitable compensation technique using the data collected in the active CT step.

3. Image reconstruction techniques

The active CT data are reconstructed using 2D filtered back projection (FBP) (Feldkamp et al., 1984) technique based on inverse Radon transform. Each reconstructed 2D slice at a given energy is then stacked to form a 3D attenuation map.

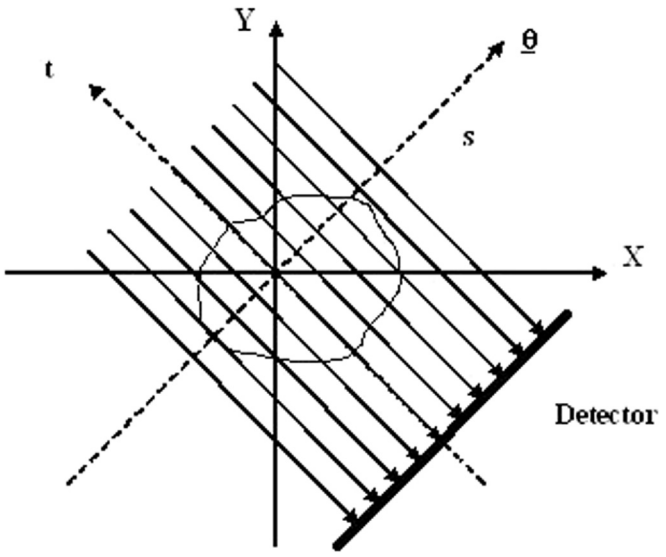

Fig. 1. A typical SPECT set-up in parallel geometry.

The passive CT data are reconstructed using iterative reconstruction technique. For iterative reconstruction, the forward projection is discretized and expressed in matrix notation as:

$$g = Af \tag{1}$$

$g = (g_1, g_2, \ldots, g_M)^T$ is the observable (measured) data, i.e. projections, $f = (f_1, f_2, \ldots\ldots, f_N)^T$ is unknown spatial density distribution of nuclear disintegration events resulting in gamma emission in the object, and A is a $M \times N$ system probability matrix (or system matrix).

3.1. System matrix

The heart of any iterative reconstruction is the system probability matrix. The system matrix A has two components – system geometry factor and system attenuation factor. The system geometry factor gives the probability that radioactive decay in a given voxel is recorded by a given detector unit/projection bin solely due to the geometrical considerations. The system attenuation factor gives the attenuation suffered by the photons in the object before reaching the detector.

To a first approximation, each element $A(i, j)$ can be expressed as:

$$A(i,j) = \frac{Area}{4\pi R_{ij}^2} \exp\left(- \sum_k \mu_k d_{ijk} \right) \tag{2}$$

Area is the exposed area of the j^{th} detector as seen by the i^{th} pixel.

R_{ij} is the distance between the i^{th} pixel and j^{th} detector.

μ_k is the attenuation coefficient of the k^{th} pixel (material) lying on the ray path joining the i^{th} pixel and j^{th} detector.

d_{ijk} is the path length in k^{th} pixel traversed by the gamma ray emitted from the i^{th} pixel and reaching the j^{th} detector.

3.2. Reconstruction: MLEM

A number of iterative techniques (Kak and Slaney, 1987; Lange and Carson 1984; Hudson and Larkin 1994; Bruyant 2002; Shepp

and Vardi 1982) are available in literature for solving the system of equations given by Eq. (1). In this work, we have used the maximum likelihood expectation maximization (MLEM) technique. It is based on the assumption that the system follows a Poisson statistics which is true in our case. Each projection g_i is expressed as a linear combination of Poisson distributed variables a_{ij}(system matrix elements).

The MLEM (Shepp and Vardi, 1982) formulation is stated mathematically as:

$$\hat{f}_j^{k+1} = \frac{\hat{f}_j^k}{\sum_{i=1}^{M} a_{ij}} \sum_{i=1}^{M} \frac{g_i}{\sum_{j'=1}^{N} a_{ij} \hat{f}_{j'}^k} a_{ij} \tag{3}$$

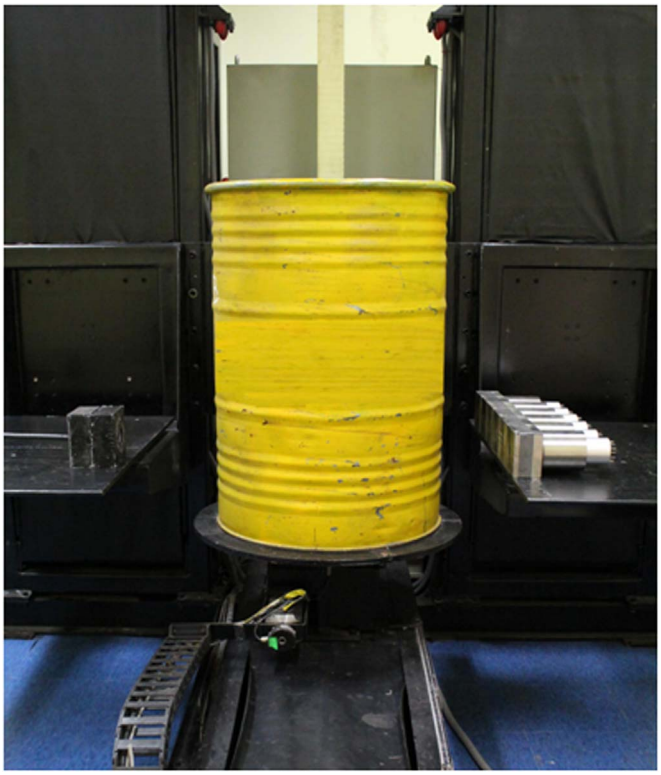

Fig. 2. Experimental set-up for A&PCT. The drum is placed on the sample stage which can rotate and translate. The active source is placed on the source stage (left) and the collimator-detector on the detector stage (right). The source-detector pair can be elevated for vertical scanning.

4. Experimental set-up

The experimental set-up is shown in Fig. 2. It consists of the following:

a) **Sample stage:** The drum is placed on a 3-axis sample manipulator. During scanning, the drum is rotated and translated whereas the source-detector pair is elevated for vertical scanning. It can scan an object of diameter 600 mm (maximum) and 1000 mm height and can handle drum weighing up to 500 kg.

b) **Active source:** An external (collimated) gamma source ^{152}Eu (33 mCi) is used for ACT. The source is housed in a portable industrial gamma radiography exposure device (ROLI-3) (www.ndt.net/article/nde-india2009/pdf/4-C-5.pdf) which is remotely operated. The collimation of the source reduces scatter and helps direct radiation towards the detector.

c) **Collimated detector assembly:** $LaBr_3$(Ce) detector (BrilLanCe™380 1″ × 1″) is used for both ACT and PCT measurements. A specially designed SS-Pb-SS collimator (Fig. 2 (inset)) with tungsten septa is used. The collimator has a square aperture of 26 mm × 26 mm divided into four equal segments using high attenuating tungsten septa of thickness 1.6 mm. For the present experiment, the length of the collimator is 50 mm which gives an effective aspect ratio (collimator length divided by collimator width) of 5:1. A detailed description of the collimator is given in (Roy et al., 2013).
A typical problem in plutonium spectroscopic measurement is the relatively high count rate from the 59.54 keV ^{241}Am gamma ray which dominates the unfiltered spectrum. If the detector is unfiltered, the americium peak will cause unnecessary deadtime. For this purpose, the detector is covered with 2 mm cadmium (followed by 0.250 mm copper) to filter the 59.54-keV gamma ray.

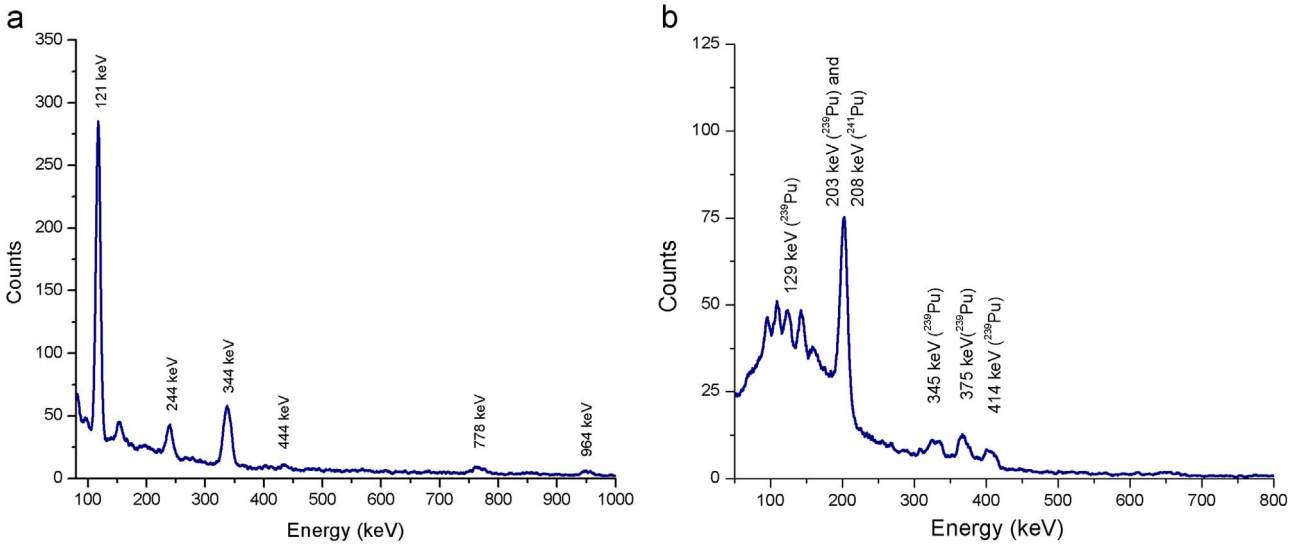

Fig. 3. Gamma spectrum recorded by $LaBr_3$(Ce) detector(a) ^{152}Eu (for active CT) (b) 93% ^{239}Pu (for passive CT). The major ^{239}Pu peaks have been labeled in (b).

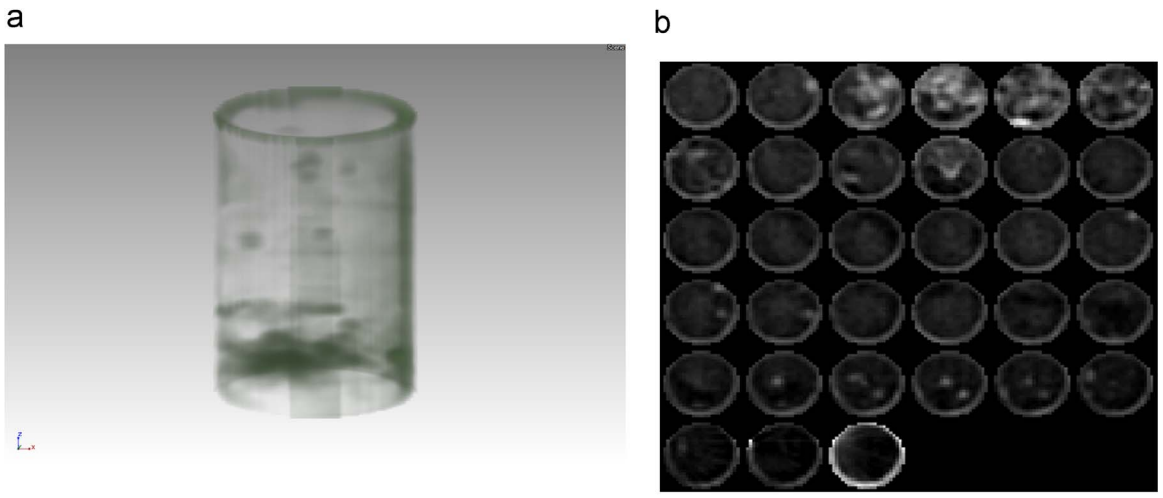

Fig. 4. (a) Reconstructed 3D attenuation map (b) Reconstructed active CT slice images at different elevations.

d) **Data acquisition system:** The spectrum from each detector is recorded using a multichannel analyzer and stored on a PC for further processing.

5. Experimental method and results

A mock waste drum (580 mm diameter and 850 mm height) is filled with cotton waste/gloves/tissues. A total of 1 g plutonium (93% ^{239}Pu) sealed in 20 aluminum cylinders (approximately 25 mm diameter and 25 mm height) containing 50 mg each are distributed at three different locations inside the drum.

5.1. Active CT

For the ACT measurement, the external gamma source and a single $LaBr_3(Ce)$ detector are used. Data was acquired at 24 lateral positions and 18 angular positions over 180° for each z-position. In the vertical direction, 33 z-positions were scanned. Each slice thickness is 25 mm. The acquisition time for each data is 10 s Fig. 3 (a) shows the gamma spectrum recorded by $LaBr_3(Ce)$ detector during Active scan. The peak area corresponding to 244 keV, 444 keV, 778 keV, 964 keV and 1407 keV were used for reconstructing the active data set and the attenuation map corresponding to these energies is reconstructed. The 344 keV peak was avoided as it interferes with the 345 keV peak from ^{239}Pu; 332.35-keV and 335.40-keV peaks from ^{241}Pu-^{237}U and cannot be discriminated. The attenuation coefficient at emission energy (414 keV) is obtained by interpolating the values from the above data set. The reconstructed attenuation map is shown in Fig. 4 (a) and (b). It can be seen that the aluminum samples with Pu can be seen in the top and middle portions of the drum (dark spheres in Fig. 4(a)). The dark region at the bottom of the drum is due to the presence of densely packed rubber gloves.

5.2. Passive CT

For the PCT measurement, the external source is removed and gamma rays emitted from within the drum are recorded by three collimated $LaBr_3(Ce)$ detectors. Fig. 3(b) shows the gamma spectrum recorded by $LaBr_3(Ce)$ detector during Passive scan. Data were acquired at 24 lateral positions and 12 angular positions over 360° for each z-position. In the vertical direction, 33 z-positions were scanned. Each slice thickness is 25 mm. The reconstructed volume is discretized on a $24 \times 24 \times 34$ grid. The 414 keV peak from ^{239}Pu is used for PCT. The reconstructed 3D volume is shown in Fig. 5. Reconstructed XY slices at different Z-positions are shown in Fig. 6. It can be seen that spatial position of the radioisotopes can be easily located.

The activity (in disintegrations per second) for each voxel is given by

$$A = \frac{C}{t\beta_\gamma \varepsilon} \tag{4}$$

where C is the reconstructed counts in the voxel, t is the acquisition time, β_γ is the branching ratio of the emitted gamma for the particular isotope and ϵ is the detector efficiency. The total activity for each distinct source is calculated by summing all the voxels in a given region. The measured activity can be converted to its mass (in gram) using the following relation:

$$m = \frac{A}{A_{sp}} \tag{5}$$

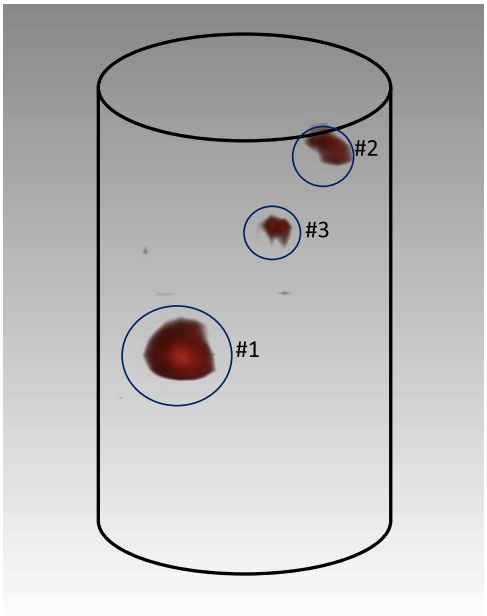

Fig. 5. Reconstructed 3D image showing activity distribution of ^{239}Pu. The drum outline is shown for illustration (b) Reconstructed passive CT slice images at different elevations.

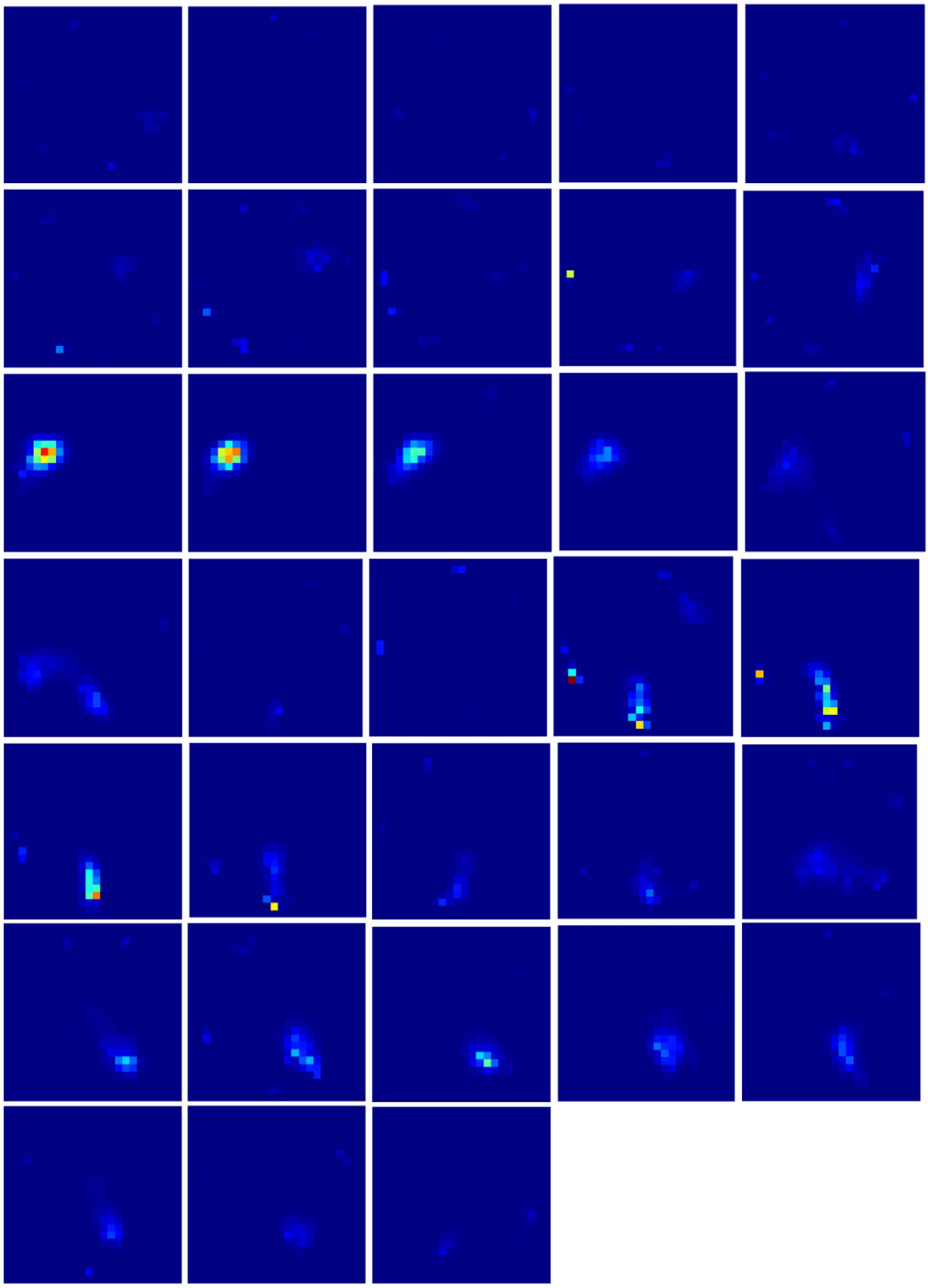

Fig. 6. Reconstructed Passive CT slice images at different elevations.

Table 1
Reconstructed ^{239}Pu mass.

Source	True ^{239}Pu mass (g)	Reconstructed ^{239}Pu mass (g)	Relative deviation (%)
#1	0.512	0.519	3.32
#2	0.232	0.233	0.43
#3	0.186	0.168	9.68

where A_{sp} is the specific activity of the radioisotope.

The reconstructed activity distribution in the images matches well with the true source activity (see Table 1). The relative deviation of the reconstructed value from the true value is defined as Relative deviation = ((Reconstructed value − True value)/True value) × 100.

6. Conclusion

An Active and Passive CT facility has been developed for detection and imaging of ^{239}Pu in waste drum. The results show that the three dimensional distribution of ^{239}Pu as well as the mass/quantity assayed matches well with the true distribution. A novel feature of the work is the use of $LaBr_3$(Ce) for imaging of ^{239}Pu which, to the best of our knowledge, is being reported for the first time. $LaBr_3$(Ce) detectors may be used for CT of radioactive waste (including transuranic waste) especially for multi-detector systems in combination with an HPGe detector in order to achieve high sensitivity.

References

Bruyant, P.P., 2002. Analytic and iterative reconstruction algorithms in SPECT. J. Nucl. Med. 43, 1343–1358.

Camp, D.C., Martz, H.E., Roberson, G.P., Decman, D.J., Bernardi, R.T., 2002. Non-destructive waste-drum assay for transuranic content by gamma-ray active and passive computed tomography. NIM-A 495, 69–83.

Feldkamp, L.A., Davis, L.C., Kress, J.W., 1984. Practical cone-beam algorithm. J. Opt. Soc. Am. 1, 612–619.

Herman, G.T., 1980. Image Reconstruction from Projections. Academic Press, New York.

Hudson, H.M., Larkin, R.S., 1994. Accelerated image reconstruction using ordered subsets of projection data. J. Nucl. Med 13, 601–609.

Kak, A.C., Slaney, M., 1987. Principles of Computerized Tomography. IEEE Press.

Lange, K., Carson, R., 1984. EM reconstruction algorithms for emission and transmission tomography. J. Comput. Assist. Tomogr. 8, 306–316.

Novikov, R.G., 2002. An inversion formula for the attenuated X-ray transformation. Ark. Math. 40, 145–167.

Roberson G.P., Martz H.E., Decman D.J., Jackson J.A., Clark D., Bernardi R.T., Camp D. C., 1998. Active and passive computed tomography for nondestructive assay In: Proceedings of the Sixth Nondestructive Assay and Nondestructive Examination Waste Characterization Conference. November 17–19, Salt Lake City, Utah pp. 359.

Roy, Tushar, Ratheesh, Jilju, Sinha, Amar, 2013. Three-dimensional SPECT imaging with LaBr3: Ce scintillator for characterization of nuclear waste. NIM- A 735, 1–6.

Roy Tushar, More, M.R., Ratheesh Jilju, Sinha Amar, 2015. A practical fan-beam design and reconstruction algorithm for Active and Passive Computed Tomography of radioactive waste barrels, NIM-A 794, 164–170.

Shepp, L.A., Vardi, Y., 1982. Maximum likelihood reconstruction for emission tomography. IEEE Trans. Med Imaging; **MI-1**, 113–122.

⟨http://dx.doi.org/www.ndt.net/article/nde-india2009/pdf/4-C-5.pdf⟩.

View publication stats